Solvation Dynamics at the Air/Water Interface with Time-Resolved Sum-Frequency Generation

Yi Rao, Nicholas J. Turro, and Kenneth B. Eisenthal*

Department of Chemistry, Columbia University, 3000 Broadway, New York, New York 10025

Received: June 8, 2010; Revised Manuscript Received: August 23, 2010

The dynamics of molecular solvation at the air/water interface has been monitored with femtosecond time-resolved pump-sum frequency generation (TR-SFG), a technique that has been shown to be feasible in the study of ultrafast rotional motions. In the work reported here, the solvation process was monitored by femtosecond photoexcitation of interfacial coumarin 314 (C314) molecules. In these experiments, the SFG signal is brought into a vibrational resonance with the carbonyl symmetric stretch of C314 by tuning the IR pulse to the carbonyl frequency by using a pump-TR-SFG probe. Two solvation time constants were obtained, 230 ± 40 fs and 2.17 ± 0.3 ps. These results are the same within experimental error as those measured in time-resolved second-harmonic generation (TR-SHG) experiments. This suggests that the solvent response is due to solvation-induced shifts of the electronic-state energies in the SFG hyperpolarizability and not significantly to solvation effects on the energy of the carbonyl vibration nor to the strength of the carbonyl vibrational transition moment. In addition, an explanation of the similar solvation dynamics of a newly created ion at the air/water interface and in bulk water, which is based on molecular-dynamics simulations (Benjamin, I. *J. Chem. Phys.* **1991**, 95 (*5*), 3698−3709), could explain the similar solvation dynamics we found for C314. The physical description is that the first solvation shell is essentially the same in bulk water and at the air/water interface.

Introduction

The solvation of solute molecules in liquids is manifested in both equilibrium and time-dependent processes. Solvation is important for the description of the chemical and physical properties of molecules in liquids, for example, electronic-state energies, acid−base equilibria, energy relaxation, and chemical-reaction dynamics.[2−4] Water, being the most important liquid, has been extensively studied in both theory and experiment.[5] The advances provided by these various investigations attest to the complexity of dynamical processes in water in that they involve the motions of water molecules that are part of water-network structures.[6−9] It is the dynamics of the formation and breaking of hydrogen bonds that underlies the rotation and translational motions of water molecules. The most commonly used experimental approach in the investigation of solvation dynamics is based on the ultrafast photoexcitation of bulk solute molecules to excited electronic states that have a charge distribution that differs from the ground electronic states, for example, different dipole moments.[10−12] The reorganization of the water molecules surrounding the excited-state molecules, effected by the changed charge distribution, is then followed by a time-delayed ultrashort probe pulse, the amplitude of which is sensitive to the change in the energy of the excited-state molecules as they evolve to their lowest solvation energy. These experiments have shown that solvation dynamics of solvtochromic organics molecules, chiefly coumarins, in bulk-phase aqueous solutions, can be characterized by three time constants.[12] A sub-50 fs component is attributed to librational water motions, and two slower time domains, one which is roughly several hundred femtoseconds and the other of the order of one picosecond, are referred to as diffusive. These latter component are generally attributed to the breaking and formation of hydrogen bonds among water molecules and water-network reorganization. There is presently no identification of the water molecular motions that can be directly used to reveal the origin of the two diffusive solvation time domains. However, there is both experimental and theoretical support of the general idea that the diffusive time domains in bulk water are connected with the making and breaking of hydrogen bonds that is attributed to the diffusive relaxation processes, ∼1 ps, and the making and breaking of hydrogen bonds, 0.5−1 ps, are similar.[7,13−16]

Just like bulk liquids are of considerable interest, the properties of that uniquely organized, molecularly thin region of matter where two bulk media make contact, namely, the interface, are also of fundamental scientific and technological significance. Unfortunately, the traditional spectroscopies, absorption, emission, IR, and Raman scattering, which are powerful methods used in the investigation of the properties of bulk liquids, have had little impact in the investigation of liquid interfaces. The reason for this is that, with the linear spectroscopies, the investigation of optical signals is generated by bulk chemical species that overwhelm the signals from the much smaller populations at the interface. Under these circumstances, nonlinear optical methods such as sum frequency generation (SFG) and second harmonic generation (SHG) emerge as alternatives, because they are interface selective; that is, no coherent SFG and SHG light is produced by molecules in isotropic bulk liquids.[17−21] SFG and SHG as second-order interactions can be employed to specifically investigate interfaces that are accessible to light, including buried interfaces.[22−35] Time-resolved SHG has been used to study solvation dynamics, rotational dynamics, electron-transfer population recovery, and other ultrafast processes.[36−50] SHG can be described as an electronic spectroscopy, and vibrational SFG can be described

* Corresponding author.

10.1021/jp105223j
Published on Web 09/17/2010

as a vibrational spectroscopy. When the incident IR light is resonant with a vibrational mode that is both Raman and IR active, SFG therefore has the sensitivity to molecular structure and molecular identity that is characteristic of linear vibrational spectroscopies.

In the SFG research reported here, the solvation dynamics is probed by tuning the frequency of the incident femtosecond IR light into resonance with the ring carbonyl symmetric stretch of C314 at the air/water interface. In earlier studies, SFG has been used to probe vibrational relaxation in molecules that have been IR-pumped to excited vibrational states in the ground electronic state.[51−53] SFG has also been used to great advantage in measuring the dynamics of vibrational energy transfer along a hydrocarbon chain.[54] In the present investigation, SFG is used to monitor the solvation dynamics of interfacial molecules. The solvation process is initiated by pumping interfacial molecules, not into ground vibronic states but rather into excited electronic states. The experiment consists of pumping C314 molecules at the air/water interface from their ground electronic state S_0, which has a permanent dipole moment of around 8 D, to the lowest excited singlet states S_1, where the dipole moment has increased to 12 D.[55]

Prior to the research presented here, there have been studies using the pump-time-resolved SHG method to investigate solvation dynamics of C314 at the neat air/water, neutral, positively charged, and negatively charged surfactant/water interfaces.[38,39,42−44,56] The solvation at the surfactant free air/water interface was slower than that in bulk water, with the slowest component being slower by a factor of two relative to the bulk value. An interesting result was the finding that the chemical composition of negatively charged surfactant head groups did not affect the solvation dynamics. The surfactants used were the negatively charged dodecyl sulfate CH_3-$(CH_2)_{11}SO^{4-}$ and the negatively charged state $CH_3(CH_2)_{16}$ COO^-. It was also found that, at the same coverage, the charged form $CH_3(CH_2)_{16}$ COO^- is four times slower than the neutral form $CH_3(CH_2)_{16}$ COOH, indicating the strong effect of surface charge on the alignment and increased hydrogen-bond order of water. A comparison of the effects of a positively charged surfactant with negatively charged surfactant molecules indicates a significant difference in their static interfacial properties, for example, orientation of C314, and in their solvation dynamics. The electrostatic interactions due to the oppositely charged surfactants would tend to align the water molecules in opposite directions and could result in the C314 molecules being located in different interfacial locations, one below the layer of surfactant head group for the positively charged DTAB and the other between the surfactant layer head groups of the negatively charged SDS. It would be of value to use SHG and SFG to gain information on the relation of the interfacial structure of the probe molecule and the surfactant with the solvation dynamics studies.

Total internal reflection time-resolved fuorescence studies of solvation at the sapphire/butanol interface found that the solvation time was roughly a factor of two slower than that in bulk butanol.[57] However, the time resolution of 60 ps limited the experiments to slow processes, and we had to consider the contributions from molecules located within the evanescent wave depth. In other total internal reflection experiments on a heptane/water interface containing ethanol molecules, it was inferred that the interfacial fluorophores are preferentially solvated by ethanol molecules.[58] Unlike the latter systems, time-resolved fluorescence studies at the interface of water/ZrO_2 nanoparticles yielded solvation times that were faster than those in bulk water.[59−61] This behavior was attributed to the disruption of the water hydrogen-bond network by the formation of the hydrogen bonds among interfacial water molecules and surface OH groups of ZrO_2. Similar effects and mechanisms were observed and proposed for solvation at the silica/butanol interface, which was found to be faster by more than a factor of three relative to bulk butanol. In a different interfacial-bulk environment, namely, the restricted space of the interior of reverse micelle, the solvation dynamics had a very slow time component, 0.1−0.3 ns.[62,63] In addition, two ultrafast components were found, one subpicosecond and the other picoseconds, both of which were slower than the corresponding time components at the air/water interface and bulk water. The effects of the surface charge at the interior reverse micelle region are consistent with the effects of charged surfactants that were found to slow the solvation dynamics at the air/water interface.

On the theoretical side, there have been notable advances in molecular-dynamics simulations of solvation dynamics at liquid interfaces. The first simulations were that of the solvation of a newly created ion at the air/water interface.[1] The dynamics in bulk water and at the interface were found to be essentially the same, which is in agreement with our experiments. The simulations showed that the solvated ion maintained its bulk solvation shell at the interface, which provides insight into why the interface and bulk values for solvation dynamics are very similar. Simulations of solvation dynamics were extended to liquid/liquid interfaces, which were found to be more complex than in bulk media or the vapor/liquid interface.[64,65] The effects of the location of the probe molecule in the interface and the effects of surface roughness on solvation dynamics were also shown to be significant in molecular-dynamics simulations. Molecular-dynamics simulations of C314 at the air/water interface yielded, when integrating over a long time interval, which will be discussed in a later section of the paper, an average solvation time of 0.79 ps, which is in agreement with our experiments.[66] The amplitud- weighted averages for the SHG experiment was found to be 0.8. To keep pace with experiments on solvation in reverse micelles, there has been a number of molecular-dynamics-simulation studies.[67,68] It was found that, in the early time domain, < 2 ps, th the solvation becomes faster as the size of the micelle increases, in agreement with experiment. It was also shown that the location of the probe with respect to the interface changed the relative contributions of the inertial and diffusive parts to the solvation dynamics of cationic groups, and the effects were to slow down the solvation and to make it strongly dependent on the micelle size. The latter effect was attributed to the location of the group in the interface, similar to what was found in solvation at self-assembled monolayer interfaces.

Experimental Section

In the following, we apply a frequency-resolved and time-resolved SFG technique. A new approach to the measurement of vibrational spectra using SFG has been developed and has proven to be successful.[31,69−72] It entails combining a spectrally broad IR pulse, which is characteristic of femtosecond IR pulses, with a spectrally narrow picosecond visible pulse. In the frequency-resolved SFG experiment, the bandwidth of the incident IR pulse is much larger than that of the vibrational resonance. Thus, vibrations within the several hundred wavenumber wide IR pulse can be detected in each pulse of the laser, which makes it possible to obtain vibrational spectra of interest more rapidly. The incident IR and visible pulses spatially overlap the interface area irradiated by the femtosecond pump pulse. In

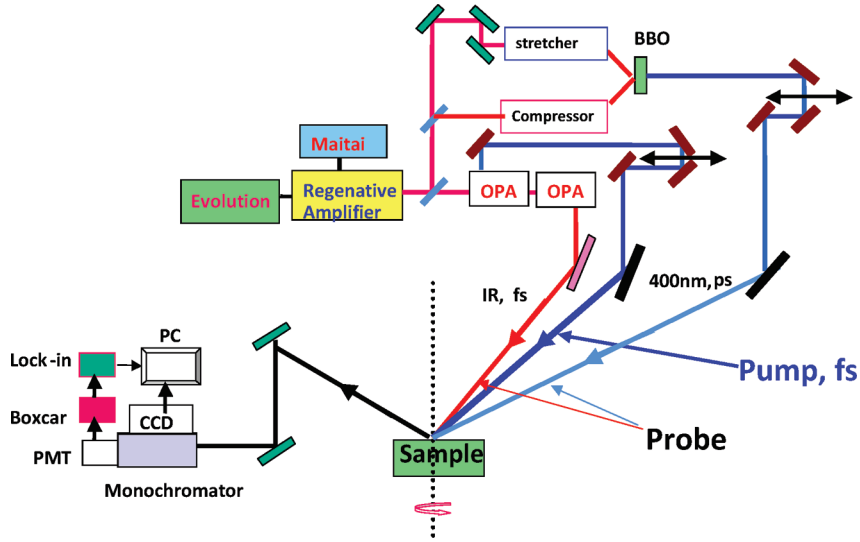

Figure 1. Schematic of time-resolved SFG experimental layout.

the time-resolved SFG experiment, the instrument response is determined by the cross-correlation time of the femtosecond IR and the femtosecond pump light.

As shown in Figure 1, an 800 nm regeneratively amplified Ti:sapphire system (Spitfire, SpectraPhysics) seeded with a MaiTai 80 MHz, 80 fs oscillator, at a repetition frequency of 1 kHz was employed in the present experiments. For the SFG measurements (800 nm and IR), a homemade pulse shaper was used to produce a 2.5 ps 800 nm pulse with a 10 cm^{-1} bandwidth. In the SFG measurements (400 nm and IR), a part of femtosecond beam from the regenerative amplifier was splitted into two parts, one being stretched to 10 ps and another being compressed to 10 ps. The stretched and compressed light was collimated spatially and temporally to 1 mm BBO (type I) to get the 400 nm picosecond light with a typical frequency resolution of 12 cm^{-1} and a typical output power of 7 μJ per pulse.[73] By using an OPA, a femtosecond 423 nm light, which serves as the pump light, was produced by fourth-harmonic generation of an idler light. With a second OPA, tunable IR light, 3−8.5 μm, with a bandwidth of 150 cm^{-1}, was generated.

The IR beam with a typical power of 1.5 μJ per pulse at 5.7 μm is focused onto the sample by a BaF_2 lens with a 100 mm focal length at an angle of 67° relative to the surface normal and a spot size of around 120 μm. The 400 nm picosecond light is focused to 210 μm spot size by a BaF_2 lens with a 250 mm focal length at an angle of 76° from the surface normal. The 423 nm pump light is focused at an angle of 70° from the surface normal with a focal spot of 800 μm, increasing the time resolution of the optical layout.

A 0.3 m spectrograph with one entry and two exits (Acton Research, three gratings including 1200 grooves/mm with 450 nm blazed, 1200 grooves/mm with 500 nm blazed, and 600 grooves/mm with 4 μm blazed) was used. The 450 nm blazed grating was chosen to measure SFG signals. One exit was configured for detecting the dispersed signal with a liquid-nitrogen cooled, back-thinned charged coupled device (CCD) camera (Roper Scientific, 1340 × 400 pixels) operating at −120 °C. The generated SFG signal was focused into the monochromator and detected by a photomultiplier tube (PMT) (Hamamatsu) when the time-profile experiments were performed. The signal from the PMT was sent into a BOXCAR average and then into a lock-in amplifier with reference to a 500 Hz chopper frequency in the pump-light arm. Two probe beams were guaranteed to overlap temporally at the maximum SFG signals in all the experiments. A translational stage and the signal sampling from the lock-in amplifier were controlled by a computer with our compiled software in Labview.

The pump−probe cross-correlation function 175 fs was measured independently by using different frequency generations of the pump beam and the IR beam at the interface. The time resolution of the detection is determined as the pump−probe cross-correlation measured by the surface pump + IR different frequency generations at the BBO or GaAs surface and therefore represents the true experimental instrument response function. It is represented by a Gaussian with a full width at half maximum of 175 fs.

The purity of coumarin 314 was checked by HPLC chromatography and used without further purification. A 15 μM solution was made by using ultrapure water (resistivity 18.2 M.cm, Millipore Corp). The Gibbs monolayers were prepared by allowing the solution to stand for 30 min prior to the start of laser experimentation in order to allow for complete monolayer formation. Experiments were typically performed at a 15 μM bulk concentration. The Teflon beakers were cleaned prior to use by immersion in freshly prepared piranha solution for 20 min and then rinsed with copious amounts of ultrapure water. The sample was contained in a shallow Teflon beaker mounted on a stage rotating at 2.5 rpm to minimize heating and degradation effects. It has been shown that coumarin 314 is a water-soluble ester that is surface active. It was found from surface-tension measurements that the surface excess of C314 is around 7 × 10^{13} molecules/cm^2 at the bulk saturation concentration of 15 μM.

Figure 2 shows the SFG spectra of a 15uM coumarin 314 aqueous solution taken at SSP polarization combinations, where the first letter indicates the polarization of the SFG light, the second letter indicates the polarization of the incident visible light, and the third letter indicates the polarization of the incident IR light. In this work, the visible beam is at 400 nm, and the IR is centered at 5.7 μm with a bandwidth of 150 cm^{-1}. The spectra shown in Figure 2 exhibit two peaks, at 1738 cm^{-1} and 1680 cm^{-1}. The main peak at 1738 cm^{-1} in the SSP polarization spectrum has been assigned to the symmetric stretching mode of −C═O in the ring of coumarin 314. To assign the main peak, we performed a control experiment on coumarin 153, the structure of which is similar to C314 because it has only one carbonyl group. The SFG spectrum of interfacial coumarin 153 shows only one peak at 1723 cm^{-1}. Therefore, we assign the

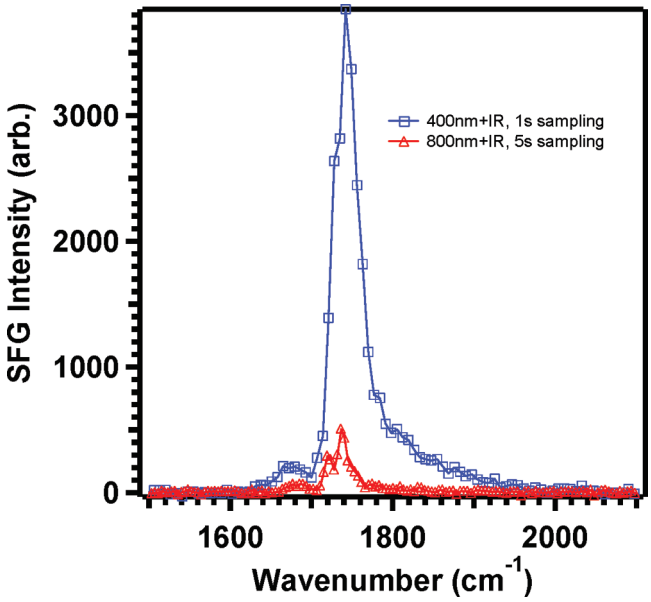

Figure 2. SSP SFG of 15 μM coumarin 314 at the air/water interface from mixing 800 nm picosecond Laser (20 μJ, s-polarization) and 400 nm picosecond Laser (7 μJ, s-polarization) with a 5.7 μm IR beam (1.5 μJ, p-polarization). The spectra were obtained from the same experimental conditions: five horizontally binned pixels; the focal spot size of the 800 nm and the 400 nm are 210um).

main peak of C314 at 1738 cm^{-1} to be the symmetric stretch of the carbonyl in the ring of C314 and the peak at 1680 cm^{-1} to be the symmetric stretch mode of the carbonyl group of the ester group of C314. In Figure 2, we see that the SFG intensity is much larger than that found when using an 800 nm picosecond pulse even though it is a factor of three more intense than that of the 400 nm pulse. An important reason for using a 400 nm picosecond laser is that the SFG signal at $\omega_{400\ nm} + \omega_{IR}$ is at a higher energy than the C314 fluorescence and thus avoids any overlap in their signals.

Results and Discussion

Here, we briefly outline the theory of SFG as it applies to interfaces. We consider two incident laser pulses, one infrared and one visible, neither of which are one- or two-photon resonant with excited electronic states of the interfacial molecules. The sum frequency intensity ($I(\omega_{SF})$) is proportional to the square of the sum of all sum frequency susceptibility terms separated into a nonresonant part $\chi^{(2)}_{NR}$ and a resonant part $\chi^{(2)}_{R}(\omega,q)$[21,22,24]

$$I^{SF}(\omega) \propto |\chi^{(2)}_{NR}e^{i\delta} + \sum_{q}^{n}\chi^{(2)}_{R}(\omega,q)|^2 \qquad (1)$$

where δ is the phase difference between nonresonant and resonant terms. In the case of dielectric interfaces, the contribution from the nonresonant parts is small compared to the resonant terms of interest.

The resonant susceptibility $\chi^{(2)}_{IJK}(\omega)$ can be expressed as[74−79]

$$\chi^{(2)}_{IJK}(\omega) = \frac{2i}{\hbar}\frac{\langle\Psi_{mv}|\alpha_m(ij)|\Psi_{mv'}\rangle\langle\Psi_{mv'}|\mu_{mm}(k)|\Psi_{mv}\rangle}{i(\omega_{mv',mv} - \omega_{IR}) + \Gamma_{mv,mv'}} \qquad (2)$$

where $\alpha_m(ij)$ represents the (ij) component of the polarizability,

$$\alpha_m(ij) = \frac{1}{\hbar}\sum_n\left[\frac{\mu_{mn}(i)\mu_{nm}(j)}{\omega_{nm} - \omega_{IR} - \omega_{UV}} + \frac{\mu_{mn}(j)\mu_{nm}(i)}{\omega_{nm} + \omega_{IR} + \omega_{UV}}\right] \qquad (3)$$

In eqs 2 and 3, $\mu_{mm}(k)$ denotes the k component of the dipole moment, Ψ_{mv} and $\Psi_{mv'}$ represent the vibrational wave functions of electronic states, and $\Gamma_{mv,mv'}$ denotes the dephasing constant.

Upon photoexcitation of interfacial C314 molecules by the pump pulse, there are contributions from both ground- and excited-state molecules. The time dependent SFG intensity is given by

$$I_{SFG}(t) \propto |\chi^{(2)}_{SSP,g}(t) + \chi^{(2)}_{SSP,e}(t) + \chi^{(2)}_{NR}|^2 \qquad (4)$$

where $\chi^{(2)}_{SSP,g}(t)$ is the time-dependent ground-state contribution and $\chi^{(2)}_{SSP,e}(t)$ is the time-dependent excited-state contribution, which evolve as the solvent reorganizes (Figure 3A). Because the SFG is a coherent optical process, the three contributions interfere constructively or destructively, depending on their relative phases. As shown in Figure 3B, the intensity of the 1738 cm^{-1} peak has decreased from its value at a time of 2 ps before the excitation pulse to that at a delay time of 1 ps after the excitation pulse. We did not see any peak shift in our time-resolved SFG experiments, which indicates that the carbonyl vibrational frequency in the excited singlet state is the same as that in the ground state within our experimental accuracy of 12 cm^{-1}. The absence of a detectable shift in the carbonyl frequency in the excited state of C314 at the air/water interface was also found to be the case for the carbonyl stretch frequency in the excited singlet state of the structurally similar coumarin 337 in bulk dichloromethane and bulk dimethyaniline.[80] Figure 4 shows TRSFG measurements of the solvation dynamics at the air/water interface. The initial drop of the SFG signal, which is fitted as a convolution of the pump pulse with the instrument response function, is due to the decrease in the C314 ground-state population and possible interference effects.

A significant finding showed that the TR-SFG and TR-SHG measurements of the diffusive solvation of C314 at the air/water interface yielded the same individual time constants, 230 ± 40 fs and 2.17 ± 0.3 ps from SFG, and 250 ± 50 fs and 2.0 ± 0.4 ps from SHG, within our experimental error. Similarly, the relative amplitudes of the individual components were found to be the same: SFG, fast component, 0.46, slow component, 0.3; SHG, fast component, 0.5, slow component, 0.24. The amplitude-averaged solvation time for the SFG result is 1.0 ps, and for SHG, it is 0.8 ps. These values are in excellent agreement with the results from the molecular-dynamics simulation of C314 solvation dynamics at the air/water interface.[66] The simulation yields an average solvation time but not the individual solvation time constants that are observed in the SFG and SHG experiments. The similar results for SFG and SHG are attributed to the solvent-induced shifts in the electronic-state energies, which are common to both measurements. From eq 2, we see that it is the Raman part of the SFG hyperpolarizability that is dependent on the energies of the electronic states. Considering the SHG hyperpolarizability, we see that it is also dependent on the energy changes, which thereby yield similar diffusive dynamics. It also reveals that the solvation dynamics at the air/water interface obtained in the SFG and SHG experiments are close to that in bulk water. For the structurally similar C343, the dynamics in bulk water has two diffusive components. The physical basis of the similar dynamics at the air/water interface and bulk water is possibly provided by the

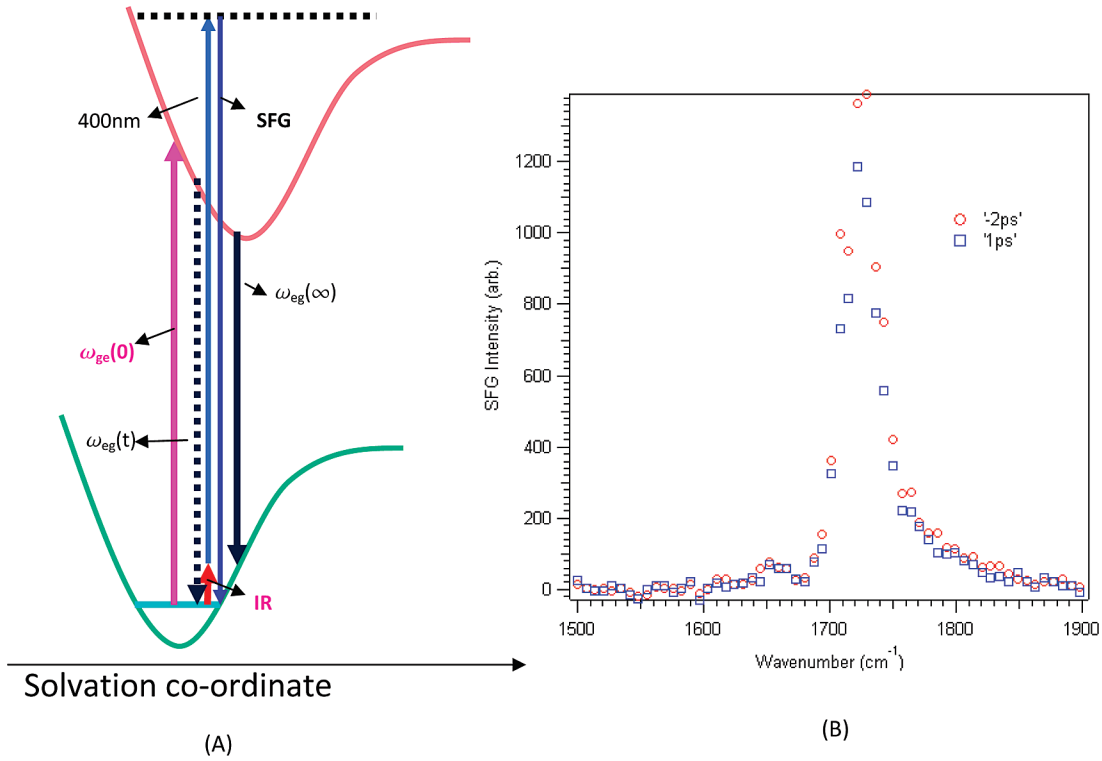

Figure 3. (A) Schematic of the energy level of coumarin 314 vs solvated coordinate. (B) SSP SFG spectra at two different delay time of −2.0 ps and 1 ps; three horizontally binned pixels, 0.5 s sampling time.

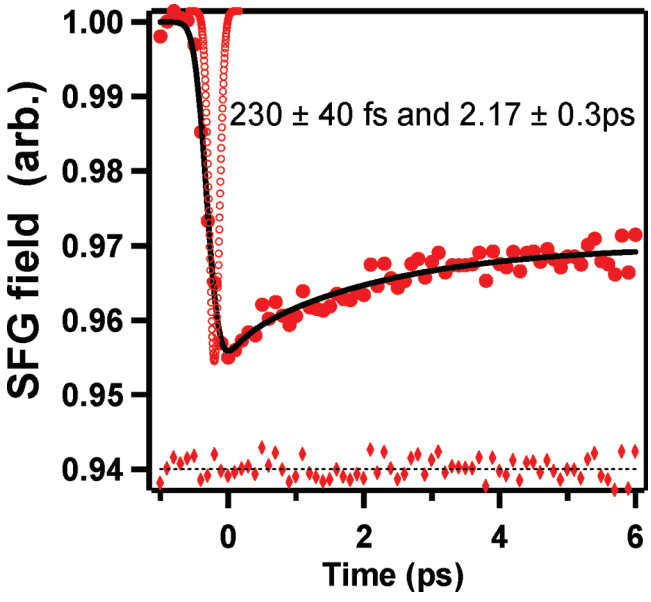

Figure 4. Electronic excited-state solvation dynamics of 15uM coumarin 314 at the air/water interface for 400 nm (S-polarization, 7 μJ) + IR (5.7u μm, p-polarization, 1.5 μJ) probe. The pump was at 423 nm (p-polarization, 0.5 μJ). The data were best fit to a sum of two exponential decays. The cross-correlation time of 180 fs was measured by mixing the pump and the IR beans to get a different frequency generation. The solid line is a fit to a biexponential giving time constants of τ_1 = 230 ± 40 fs and τ_2 =2.17 ± 0.3 ps.

molecular-dynamics simulations of solvation in the bulk and interface, where it was found that the first water shell surrounding the probe species in bulk water remains intact at the air/water interface. If it is the motions of the first water shell that are chiefly responsible for the diffusive solvation dynamics;then, the physical origin for the similar dynamics observed in bulk water and at the air/water interface is reasonable. Although the first water shell for C314 at the air/water interface and in bulk water could be the same, the friction experienced in rotational motions is considerably different at the interface and in bulk media and thus involves not only the first shell but also a more extensive reorganization of the surrounding water network. One latest SHG and SFG measurements of out of plane interfacial motions of C314 are slower at the interface by more than 100 ps than in bulk water.[73,81]

Conclusions

Femtosecond time-resolved vibrational SFG has been used to measure the solvation dynamics of the organic dye molecule coumarin 314 at the air/water interface. On the basis of the similar dynamics obtained from SFG and SHG measurements, it is suggested that it is the solvation-induced shifts in the electronic-state energies, common to both TR-SFG and TR-SHG measurements, that are responsible for the similar dynamics. Thus, it is the Raman part, not the vibrational transition part of the SFG hyperpolarizability, that changes as solvation occurs. An explanation of the similar solvation dynamics of a newly created ion at the air/water interface and in bulk water, which is based on molecular-dynamics simulations, could explain the similar solvation dynamics that we found for C314. The physical description is that the first solvation shell is essentially the same in bulk water and at the air/water interface.

Acknowledgment. The authors thank the National Science Foundation, the Chemical Sciences, Geosciences and Biosciences Division, and Office of Basic Energy Sciences, Office of Science, US Department of Energy, and DTRA (W911NF-07-1-0116). The authors also thank the National Science Foundation for generous support of this research through Grants CHE-07-17518 and DRM 02-13774.

References and Notes

(1) Benjamin, I. *J. Chem. Phys.* **1991**, *95* (5), 3698–3709.
(2) *Ultrafast reaction dynamics and solvent effects: Royaumont, France 1993*; American Institute of Physics: New York, 1994; p 564.
(3) *Ultrafast dynamics of chemical systems*; Kluwer Academic Publishers: Dordrecht; Boston, 1994; p 385.
(4) Dogonadze, R. R. *The chemical physics of solvation*; Elsevier: Amsterdam, 1985; p 3.
(5) Marechal, Y. *The hydrogen bond and the water molecule: the physics and chemistry of water, aqueous and bio media*, 1st ed.; Elsevier: Amsterdam, 2007; p 318.
(6) Gale, G. M.; Gallot, G.; Hache, F.; Lascoux, N. *Phys. Rev. Lett.* **1999**, 1–4.
(7) Lawrence, C. P.; Skinner, J. L. *Chem. Phys. Lett.* **2003**, *369*, 472–477.
(8) Tokmakoff, A. *J. Chem. Phys. A* **2003**, *107*, 5258–5279.
(9) Yeremenko, S.; Pshenichnikov, M. S.; Wiersma, D. A. *Chem. Phys. Lett.* **2003**, *369*, 107–113.
(10) Kahlow, M. A.; Jarzeba, W.; Kang, T. J.; Barbara, P. F. *J. Chem. Phys.* **1989**, *90* (1), 151–158.
(11) Nagarajan, V.; Brearley, A. M.; Kang, T. J.; Barbara, P. F. *J. Chem. Phys.* **1987**, *86* (6), 3183–3196.
(12) Jimenez, R.; Fleming, G. R.; Kumar, P. V.; Maroncelli, M. *Nature* **1994**, *369* (6480), 471–473.
(13) Asbury, J. B.; Steinel, T.; Fayer, M. D. *J. Phys. Chem. B* **2004**, *108* (21), 6544–6554.
(14) Steinel, T.; Asbury, J. B.; Zheng, J. R.; Fayer, M. D. *J. Phys. Chem. A* **2004**, *108* (50), 10957–10964.
(15) Woutersen, S.; Bakker, H. J. *Phys. Rev. Lett.* **1999**, *83* (10), 2077–2080.
(16) Yeremenko, S.; Pshenichnikov, M. S.; Wiersma, D. A. *Chem. Phys. Lett.* **2003**, *369* (1−2), 107–113.
(17) Bloembergen, N., *Nonlinear optics; a lecture note and reprint volume [by] N. Bleombergen*; W.A. Benjamin: New York, 1965; p 222.
(18) Boyd, R. W. *Nonlinear optics*; Academic Press: Boston, 1992; p 439.
(19) Butcher, P. N. *The elements of nonlinear optics*; Cambridge University Press: Cambridge, 1990; p 344.
(20) Mills, D. L. *Nonlinear optics: basic concepts*; Springer-Verlag: Berlin, 1991; p 184.
(21) Shen, Y. R. *The principles of nonlinear optics*; Wiley: New York, 1984; p 563.
(22) Shen, Y. R. *Nature* **1989**, *337* (6207), 519–525.
(23) Eisenthal, K. B. *Chem. Rev.* **1996**, *96* (4), 1343–1360.
(24) Miranda, P. B.; Shen, Y. R. *J. Phys. Chem. B* **1999**, *103* (17), 3292–3307.
(25) Richmond, G. L. *Chem. Rev.* **2002**, *102* (8), 2693–2724.
(26) Chen, Z.; Shen, Y. R.; Somorjai, G. A. *Annu. Rev. Phys. Chem.* **2002**, *53*, 437–465.
(27) Liu, D. F.; Ma, G.; Levering, L. M.; Allen, H. C. *J. Phys. Chem. B* **2004**, *108* (7), 2252–2260.
(28) Baldelli, S.; Schnitzer, C.; Shultz, M. J.; Campbell, D. J. *J. Phys. Chem. B* **1997**, *101* (49), 10435–10441.
(29) Simonelli, D.; Baldelli, S.; Shultz, M. J. *Chem. Phys. Lett.* **1998**, *298* (4−6), 400–404.
(30) Wang, H. F.; Gan, W.; Lu, R.; Rao, Y.; Wu, B. H. *Int. Rev. Phys. Chem.* **2005**, *24* (2), 191–256.
(31) Rao, Y.; Comstock, M.; Eisenthal, K. B. *J. Phys. Chem. B* **2006**, *110* (4), 1727–1732.
(32) Geiger, F. M. *Annu. Rev. Phys. Chem.* **2009**, *60*, 61–83.
(33) Kataoka, S.; Cremer, P. S. *J. Am. Chem. Soc.* **2006**, *128* (16), 5516–5522.
(34) Fourkas, J. T.; Walker, R. A.; Can, S. Z.; Gershgoren, E. *J. Phys. Chem. C* **2007**, *111* (25), 8902–8915.
(35) Conboy, J. C.; Kriech, M. A. *Anal. Chim. Acta* **2003**, *496* (1−2), 143–153.
(36) Castro, A.; Sitzmann, E. V.; Zhang, D.; Eisenthal, K. B. *J. Phys. Chem.* **1991**, *95* (18), 6752–6753.
(37) Zimdars, D.; Dadap, J. I.; Eisenthal, K. B.; Heinz, T. F. *J. Phys. Chem. B* **1999**, *103* (17), 3425–3433.
(38) Zimdars, D.; Dadap, J. I.; Eisenthal, K. B.; Heinz, T. F. *Chem. Phys. Lett.* **1999**, *301* (1−2), 112–120.
(39) Benderskii, A. V.; Eisenthal, K. B. *J. Phys. Chem. B* **2000**, *104* (49), 11723–11728.
(40) Benderskii, A. V.; Eisenthal, K. B. *J. Phys. Chem. B* **2001**, *105*, 6698–6703.
(41) Shang, X. M.; Benderskii, A. V.; Eisenthal, K. B. *J. Phys. Chem. B* **2001**, *105* (47), 11578–11585.
(42) Zimdars, D.; Eisenthal, K. B. *J. Phys. Chem. B* **2001**, *105*, 3993–4002.
(43) Benderskii, A. V.; Eisenthal, K. B. *J. Phys. Chem. A* **2002**, *106* (33), 7482–7490.
(44) Benderskii, A. V.; Henzie, J.; Basu, S.; Shang, X. M.; Eisenthal, K. B. *J. Phys. Chem. B* **2004**, *108* (37), 14017–14024.
(45) McArthur, E. A.; Eisenthal, K. B. *J. Am. Chem. Soc.* **2006**, *128* (4), 1068–1069.
(46) Shang, X. M.; Nguyen, K.; Rao, Y.; Eisenthal, K. B. *J. Phys. Chem. C* **2008**, *112* (51), 20375–20381.
(47) Meech, S. R.; Yoshihara, K. *Photochem. Photobiol.* **1991**, *53* (5), 627–632.
(48) Steinhurst, D. A.; Baronavski, A. P.; Owrutsky, J. C. *J. Phys. Chem. B* **2002**, *106* (12), 3160–3165.
(49) Antoine, R.; Tamburello-Luca, A. A.; Hebert, P.; Brevet, P. F.; Girault, H. H. *Chem. Phys. Lett.* **1998**, *288* (1), 138–146.
(50) Yamaguchi, S.; Tahara, T. *J. Chem. Phys.* **2006**, *125* (19), .
(51) Harris, A. L.; Rothberg, L. *J. Chem. Phys.* **1991**, *94* (4), 2449–2457.
(52) McGuire, J. A.; Shen, Y. R. *Science* **2006**, *313* (5795), 1945–1948.
(53) Sovago, M.; Campen, R. K.; Wurpel, G. W. H.; Muller, M.; Bakker, H. J.; Bonn, M. *Phys. Rev. Lett.* **2008**, *100* (17), .
(54) Wang, Z. H.; Carter, J. A.; Lagutchev, A.; Koh, Y. K.; Seong, N. H.; Cahill, D. G.; Dlott, D. D. *Science* **2007**, *317* (5839), 787–790.
(55) Moylan, C. R. *J. Phys. Chem.* **1994**, *98* (51), 13513–13516.
(56) Benderskii, A. V.; Eisenthal, K. B. *J. Phys. Chem. B* **2001**, *105*, 6698–6703.
(57) Yanagimachi, M.; Tamai, N.; Masuhara, H. *Chem. Phys. Lett.* **1992**, *200*, 0–5.
(58) Yamashita, T.; Uchida, T.; Fukushima, T.; Teramae, N. *J. Phys. Chem. B* **2003**, *107* (20), 4786–4792.
(59) Martins, L. R.; Skaf, M. S.; Ladanyi, B. M. *J. Phys. Chem. B* **2004**, *108* (51), 19687–19697.
(60) Pant, D.; Levinger, N. E. *Spectroscopy* **1998**, 200–206.
(61) Pant, D.; Levinger, N. E. *J. Phys. Chem.* **1999**, *103*, 7846–7852.
(62) Levinger, N. E. *Curr. Opin. Colloid Interface Sci.* **2000**, *5* (1−2), 118–124.
(63) Willard, D. M.; Levinger, N. E. *J. Phys. Chem. B* **2000**, *104* (47), 11075–11080.
(64) Michael, D.; Benjamin, I. *J. Phys. Chem.* **1995**, *99* (46), 16810–16813.
(65) Michael, D.; Benjamin, I. *J. Chem. Phys.* **2001**, *114* (6), 2817–2824.
(66) Pantano, D. A.; Laria, D. *J. Phys. Chem. B* **2003**, *107*, 2971–2977.
(67) Faeder, J.; Ladanyi, B. M. *J. Phys. Chem. B* **2001**, *105* (45), 11148–11158.
(68) Faeder, J.; Ladanyi, B. M. *J. Phys. Chem. B* **2005**, *109* (14), 6732–6740.
(69) Richter, L. J.; Petralli-Mallow, T. P.; Stephenson, J. C. *Opt. Lett.* **1998**, *23* (20), 1594–1596.
(70) Hommel, E. L.; Ma, G.; Allen, H. C. *Anal. Sci.* **2001**, *17* (11), 1325–1329.
(71) Rao, Y.; Subir, M.; McArthur, E. A.; Turro, N. J.; Eisenthal, K. B. *Chem. Phys. Lett.* **2009**, *477* (4−6), 241–244.
(72) Rao, Y.; Turro, N. J.; Eisenthal, K. B. *J. Phys. Chem. C* **2009**, *113* (32), 14384–14389.
(73) Rao, Y.; Song, D. H.; Turro, N. J.; Eisenthal, K. B. *J. Phys. Chem. B* **2008**, *112* (43), 13572–13576.
(74) Lin, S. H.; Hayashi, M.; Lin, C. H.; Yu, J.; Villaeys, A. A.; Wu, G. Y. C. *Mol. Phys.* **1995**, *84* (3), 453–468.
(75) Lin, S. H.; Hayashi, M.; Islampour, R.; Yu, J.; Yang, D. Y.; Wu, G. Y. C. *Physica B* **1996**, *222* (1−3), 191–208.
(76) Liao, D. W.; Hayashi, M.; Liu, W. K.; Islampour, R.; Yang, T. S.; Lin, S. H.; Wu, G. Y. C.; Yu, J. *J. Korean Phys. Soc.* **1998**, *32* (3), 320–325.
(77) Hayashi, M.; Lin, S. H.; Raschke, M. B.; Shen, Y. R. *J. Phys. Chem. A* **2002**, *106* (10), 2271–2282.
(78) Raschke, M. B.; Hayashi, M.; Lin, S. H.; Shen, Y. R. *Chem. Phys. Lett.* **2002**, *359* (5−6), 367–372.
(79) Hayashi, M.; Lin, S. H.; Shen, Y. R. *J. Phys. Chem. A* **2004**, *108* (39), 8058–8076.
(80) Wang, C. F.; Akhremitchev, B.; Walker, G. C. *J. Phys. Chem. A* **1997**, *101* (15), 2735–2738.
(81) Nguyen, K. T.; Shang, X. M.; Eisenthal, K. B. *J. Phys. Chem. B* **2006**, *110* (40), 19788–19792.

JP105223J